Article

Synthesis and Size-Dependent Exchange Bias in Inverted Core–Shell MnO|Mn$_3$O$_4$ Nanoparticles

German Salazar-Alvarez, Jordi Sort, Santiago Suriach, M. Dolors Bar, and Josep Nogus

J. Am. Chem. Soc., **2007**, 129 (29), 9102-9108• DOI: 10.1021/ja0714282 • Publication Date (Web): 27 June 2007

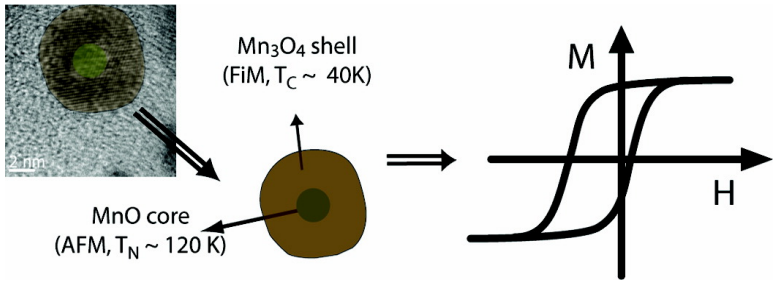

More About This Article

Additional resources and features associated with this article are available within the HTML version:

- Supporting Information
- Links to the 7 articles that cite this article, as of the time of this article download
- Access to high resolution figures
- Links to articles and content related to this article
- Copyright permission to reproduce figures and/or text from this article

View the Full Text HTML

J|A|C|S
ARTICLES
Published on Web 06/27/2007

Synthesis and Size-Dependent Exchange Bias in Inverted Core−Shell MnO|Mn_3O_4 Nanoparticles

German Salazar-Alvarez,*,† Jordi Sort,‡,§ Santiago Suriñach,§ M. Dolors Baró,§ and Josep Nogués†,‡

Contribution from the Institut Català de Nanotecnologia, Institució Catalana de Recerca i Estudis Avançats, and Departament de Física, Campus UAB, Universitat Autònoma de Barcelona, E-08193 Bellaterra, Barcelona, Spain

Received February 28, 2007; E-mail: gsa.icn@gmail.com

Abstract: Core−shell nanoparticles of MnO|Mn_3O_4 with average particle sizes of 5−60 nm, composed of an antiferromagnetic (AFM) core and a ferrimagnetic (FiM) shell, have been synthesized and their magnetic properties investigated. The core−shell structure has been generated by the passivation of the MnO cores, yielding an *inverted* AFM-core|FiM-shell system, as opposed to the typical FM-core|AFM-shell. The exchange-coupling between AFM and FiM gives rise to an enhanced coercivity of ∼8 kOe and a loop shift of ∼2 kOe at 10 K, i.e., exchange bias. The coercivity and loop shift show a non-monotonic variation with the core diameter. The large coercivity and the loop shift are ascribed to the highly anisotropic Mn_3O_4 and size effects of the AFM (i.e., uncompensated spins, AFM domains, and size-dependent transition temperature).

Introduction

Magnetic nanoparticles have attracted the interest of researchers and industry in recent years due to the large number of current and foreseen applications, including catalytic, magnetic, electronic, and biomedical types.[1] Particularly, since the report on the use of exchange bias to overcome the superparamagnetic limit,[2] the amount of experimental and theoretical work on core−shell exchange-coupled nanoparticles has increased considerably.[3−5] Exchange coupling, or exchange bias, occurs typically when a ferromagnetic (FM) material (or ferrimagnetic, FiM) in physical contact with an antiferromagnetic (AFM) material is cooled below the Curie temperature, T_C, and above the Néel temperature, T_N, such that $T_N < T < T_C$, under a static magnetic field, H_{FC}, to a $T < T_N$. Hence, when cooling through T_N, the interface spins in the AFM tend to couple to the spins in the FM. This interface coupling brings about a range of new phenomena, such as a shift of the hysteresis loop along the direction of the field axis due to an induced unidirectional anisotropy or an increase of the coercivity due to an enhanced anisotropy.[3,6,7] Most of the studied exchange-biased nanoparticle systems prepared by soft chemical methods are composed of transition metal ferromagnetic cores and the corresponding passivation shell, such as Co|CoO,[8] Ni|NiO,[9] (Co,Ni)|(Co,-Ni)O,[10] Fe|Fe_xO_y,[11] or Mn|Mn_xO_y,[12] or oxides with different oxidation states, as in CrO_2|Cr_2O_3[13] or Fe_3O_4|α-Fe_2O_3 and Fe_3O_4|FeO.[14] Recently, controlled core−shell nanoparticles such as $SrFe_{12}O_{19}$|CoO,[15] $CoFe_2O_4$|MnO,[16] or FePt|MnO[17] have also been reported. In this regard, manganese oxide nanoparticles have been studied as model magnetic systems due to their spin-only contribution to the magnetic anisotropy.[18] There are a number of manganese bulk compounds arising from the various oxidation states of manganese, where among the most relevant

† Institut Català de Nanotecnologia.
‡ Institució Catalana de Recerca i Estudis Avançats.
§ Departament de Física.

(1) (a) Gubin, S. P.; Koksharov, Y. A.; Khomutov, G. B.; Yurkov, G. Y. *Russ. Chem. Rev.* **2005**, *74*, 489. (b) Willard, M. A.; Kurihara, L. K.; Carpenter, E. E.; Calvin, S.; Harris, V. G. *Int. Mater. Rev.* **2004**, *49*, 125. (c) Batlle, X.; Labarta, A. *J. Phys. D: Appl. Phys.* **2002**, *35*, R15. (d) Tartaj, P.; Morales, M. P.; Veintemillas-Verdager, S.; González-Carreño, T.; Serna, C. J. *J. Phys. D: Appl. Phys.* **2003**, *36*, R182. (e) Häfeli, U.; Schütt W.; Teller J.; Zborowski M. *Scientific and clinical applications of magnetic carriers;* Kluwer Academic Press/Plenum Publishers: Amsterdam, 1997. (f) Pearton, S. J.; Abernathy, C. R.; Overberg, M. E.; Thaler, G. T.; Norton, D. P.; Theodoropoulou, N.; Hebard, A. F.; Park, Y. D.; Ren, F.; Kim, J.; Boatner, L. A. *J. Appl. Phys*. **2003**, *93*, 1.
(2) (a) Skumryev, V.; Stoyanov, S.; Zhang, Y.; Hadjipanayis, G.; Givord, D.; Nogués, J. *Nature* **2003**, *423*, 850. (b) Eisenmenger, J.; Schuller, I. K. *Nat. Mater.* **2003**, *2*, 437.
(3) Nogués, J.; Sort, J.; Langlais, V.; Skumryev, V.; Suriñach, S.; Muñoz, J. S.; Baró, M. D. *Phys. Rep.* **2005**, *422*, 65.
(4) Darling, S. B.; Bader, S. D. *J. Mater. Chem.* **2006**, *15*, 4189.
(5) (a) Iglesias, O.; Labarta, A.; Batlle, X. *J. Nanosci. Nanotechnol.* **2007**, arXiv: cond-mat/0607716. (b) Trohidou, K. N. In *Surface Effects in Magnetic Nanoparticles*; Fiorani, D., Ed.; Springer Verlag: New York, 2005.
(6) Nogués, J.; Schuller, I. K. *J. Magn. Magn. Mater.* **1999**, *192*, 203.
(7) Berkowitz, A.E.; Takano, K. *J. Magn. Magn. Mater.* **1999**, *200*, 552.
(8) (a) Gangopadhyay, S.; Hadjipanayis, G. C.; Sorensen, C. M.; Klabunde, K. J. *J. Appl. Phys.* **1993**, *73*, 6964. (b) Tracy, J. B.; Weiss, D. N.; Dinega, D. P.; Bawendi, M. G. *Phys. Rev. B* **2005**, *72*, 064404.
(9) Lee, I. S.; Lee, N.; Park, J.; Kim, B. H.; Yi, Y. W.; Kim, T.; Kim, T. K.; Lee, I. H.; Paik, S. R.; Hyeon, T. *J. Am. Chem. Soc.* **2006**, *128*, 10658.
(10) Luna, C.; Morales, M. P.; Serna, C. J.; Vazquez, M. *Nanotechnology* **2004**, *15*, S293.
(11) Zheng, R. K.; Wen, G. H.; Zhang, X. X. *Phys. Rev. B* **2004**, *69*, 214431.
(12) Si, P. Z.; Li, D.; Lee, J. W.; Choi, C. J.; Zhang, Z. D.; Geng, D. Y.; Brück, E. *Appl. Phys. Lett.* **2005**, *87*, 133122.
(13) (a) Yu, M. H.; Devi, P. S.; Lewis, L. H.; Oouma, P.; Parise, J. B.; Gambino, R. J. *Mater. Sci. Eng. B* **2003**, *103*, 262. (b) Zheng, R. K.; Liu, H.; Wang, X. X. *Appl. Phys. Lett.* **2004**, *84*, 702.
(14) (a) Redl, F. X.; Black, C. T.; Papaefthymiou, G. C.; Sandstrom, R. L.; Yin, M.; Zheng, H.; Murria, C. B.; O'Brien, S. P. *J. Am. Chem. Soc.* **2004**, *126*, 14583. (b) Bae, C. J.; Hwang, Y.; Park, J.; An, K.; Lee, Y.; Lee, J.; Hyeon, T.; Park, J. G. *J. Magn. Magn. Mater*. **2007**, *310*, E806.
(15) Liu, X. S.; Gu, B. X.; Zhong, W.; Jiang, Du, Y. W. *Appl. Phys. A* **2003**, *77*, 673.
(16) Masala, O.; Seshadri, R. *J. Am. Chem. Soc*. **2005**, *127*, 9354.
(17) Rutledge, R. D.; Morris, W. H.; Wellons, M. S.; Gai, Z.; Shen, J.; Bentley, J.; Wittig, J. E.; Lukehart, C. M. *J. Am. Chem. Soc.* **2006**, *128*, 14210.

 10.1021/ja0714282 CCC: $37.00

are the antiferromagnetic MnO and MnO_2 and the ferrimagnetic Mn_3O_4 and γ-Mn_2O_3. Manganese oxide nanoparticles (and nanowires) have been prepared by a number of methods, including aqueous and organic syntheses, thermal evaporation, thermolysis, sol−gel, etc.[19,20] Special interest has been paid to the synthetic methods which yield such nanoparticles with a narrow size distribution and controlled sizes or shapes.[20] Despite the recent efforts in the magnetic characterization of these novel materials, the exchange-coupling between the AFM MnO and its passivation compound, FiM Mn_3O_4, has been largely overlooked.

In this work, we systematically study the variation of magnetic properties of MnO|Mn_3O_4 antiferromagnetic−ferrimagnetic core−shell nanoparticles with a narrow size distribution as a function of the diameter of the antiferromagnetic core, as opposed to the typical core−shell ferromagnetic−antiferromagnetic case, where the size of the FM core is varied.

Experimental Section

The particles with tailored sizes were prepared by adding 1.5 mmol of manganese(II) acetylacetonate ($Mn(acac)_2$, Aldrich) and 1.5 mmol of 1,2-hexadecanediol (HDD, Aldrich) (unless otherwise stated) to 30 dm^3 of dibenzyl ether (DBE, Aldrich) in a 100 dm^3 Schlenk flask under an inert argon atmosphere, followed by the addition of oleylamine, to achieve a surfactant-to-metal molar ratio, [S]:[M], of either 2 or 20. The slurry was mechanically stirred and heated to a given temperature, T, in the range 150−290 °C. The reaction was allowed to proceed under reflux with a residence time, τ, of 10−60 min and then removed from the heating source and quenched by the addition of cold solvent. The exact values for the synthesis of particles with different sizes are given in Table 1. The reaction vessel was removed from the heating source and allowed to cool to room temperature before being exposed to air, where the passivation occurred. The particles were washed from the reaction media by subsequent steps of precipitation under ethanol, centrifugation, and re-dispersion in hexane. The global microstructure of the particles was characterized by X-ray diffraction (XRD) using a Philips 3050 diffractometer with Cu Kα radiation. The measurements were carried out in the range 30−120°, with a step size of 0.04° and a collection time of 40 s. Quantitative analysis of the XRD data was undertaken with a full pattern fitting procedure based on the Rietveld[21] method using the program MAUD.[22] The particles were imaged with a high-resolution transmission electron microscope (HRTEM, JEOL-2011) operating at an accelerating voltage of 200 kV. Particle size, D_P, and its standard deviation, σ_P, were obtained by calculating the number average by manually measuring the equivalent diameter of >200 particles from TEM micrographs. Selected-area electron diffraction (SAED), in conjunction with HRTEM analyses, was used to determine the local crystallographic phases. The magnetic properties of the samples were measured with a superconducting quantum interference device (SQUID) magnetometer using a maximum applied field of 70 kOe. In the case of the field-cooling procedures, the samples were cooled from 150 K under an applied static field of 50 kOe (unless otherwise stated). X-ray photoelectron spectroscopy (XPS) analyses were performed in a PHI 5500 multitechnique system (Physical Electronics Division, Perkin-Elmer Inc.) with a monochromatic X-ray source (Al Kα line of 1486.6 eV and 350 W), placed perpendicular to the analyzer axis and calibrated using the Ag $3d_{5/2}$ line with a full width at half-maximum (fwhm) of 0.8 eV. The charging effect on the spectra was corrected by setting the signal of adventitious carbon to 285 eV.

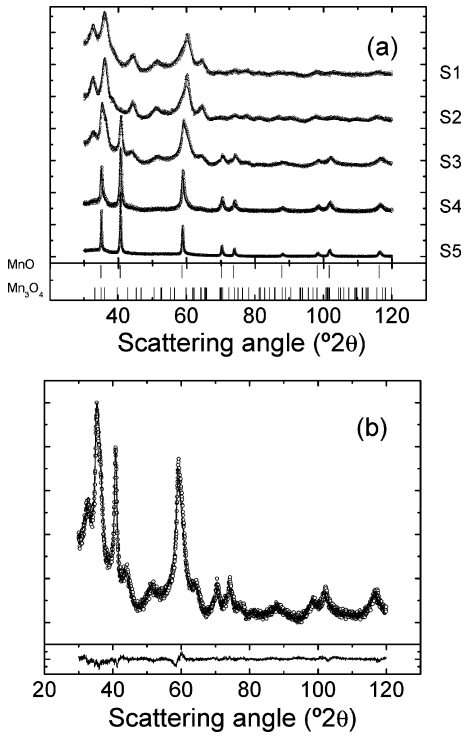

Figure 1. (a) XRD diffractograms of all the samples, S1−S5. The lines below show the position of the reflections corresponding to cubic MnO phase (JCPDS Card No. 07-0230) and the tetragonal Mn_3O_4 phase (JCPDS Card No. 24-0734). (b) Detailed view of the experimental (symbols) and fitted pattern (line) of sample S3. The line below corresponds to the difference between the two patterns.

Table 1. Description of the Synthesis Conditions for the Studied Samples and Some of Their Structural Parameters As Determined by XRD[a]

sample	[S]:[M] (mol/mol)	$[Mn^{II}]$ (mol/dm^3)	T (°C)	τ (min)	$\phi_{Mn_3O_4}$	ϕ_{MnO}	$t_{Mn_3O_4}$ (nm)	D_{MnO} (nm)
S1	20	0.05	150	10	1	0	4.8	0
S2	20	0.05	200	30	0.994	0.006	5.9	2.2
S3	20	0.05	290	60	0.870	0.130	5.7	12
S4	2	0.03	290	60	0.754	0.246	5.7	18
S5	2	0.05	290	60	0.263	0.737	5.7	50

[a] $\phi_{Mn_3O_4}$ and ϕ_{MnO} represent the volume fraction of Mn_3O_4 and MnO, respectively. $t_{Mn_3O_4}$ and D_{MnO} are the crystallite sizes of Mn_3O_4 and MnO, respectively.

Results

Figure 1 shows the experimental and calculated diffractograms obtained for the samples indicated in Table 1. The diffractograms reveal that there is a gradual intensity increase

(18) Golosovsky, I. V.; Mirebeau, I.; André, G.; Kurdykov, D. A.; Kumzerov, Y. A.; Vakhrushev, S. B. *Phys. Rev. Lett.* **2001**, *86*, 5783.
(19) (a) Moore, T. E.; Ellis, M.; Selwood, P. W. *J. Am. Chem. Soc.* **1950**, *72*, 856. (b) Winkler, E.; Zysler, R. D.; Fiorani, D. *Phys. Rev. B* **2004**, *70*, 174406. (c) Ghosh, M.; Biswas, K.; Sundaresan, A.; Rao, C. N. R. *J. Mater. Chem.* **2006**, *16*, 106. (d) Chang, Y. Q.; Xu, X. Y.; Luo, X. H.; Chen, C. P.; Yu, D. P. *J. Cryst. Growth* **2004**, *264*, 232. (e) Chang, Y. Q.; Yu, D. P.; Long, Y.; Xu, J.; Luo, X. H.; Ye, R. C. *J. Cryst. Growth* **2005**, *279*, 88. (f) Folch, B.; Larionova, J.; Guari, Y.; Guérin, C.; Mehdi, A.; Reyé, C. *J. Mater. Chem.* **2004**, *14*, 2703. (g) Na, C. W.; Han, D. S.; Kim, D. S.; Park, J.; Jeon, Y. T.; Lee, G.; Jung, M. H. *Appl. Phys. Lett.* **2005**, *87*, 142504.
(20) (a) Rockenberger, J.; Scher, E. C.; Alivisatos, A. P. *J. Am. Chem. Soc.* **1999**, *121*, 11595. (b) Lee, G. H.; Huh, S. H.; Jeong, J. W.; Choi, B. J.; Kim, S. H.; Ri, H. C. *J. Am. Chem. Soc.* **2002**, *124*, 12094. (c) Yin, M.; O'Brien, S. *J. Am. Chem. Soc.* **2003**, *125*, 10180. (d) Jana, N. R.; Chen, Y.; Peng, X. *Chem. Mater.* **2004**, *16*, 3931. (e) Park, J.; Kang, E.; Bae, C. J.; Park, J. G.; Noh, H. J.; Kim, J. Y.; Park, J. H.; Park, H. M.; Hyeon, T. *J. Phys. Chem. B* **2004**, *108*, 13594. (f) Seo, W. S.; Jo, H. H.; Lee, K.; Kim, B.; Oh, S. J.; Park, J. T. *Angew. Chem.* **2004**, *116*, 1135. (g) Park, J.; An, K.; Hwang, Y.; Park, J. G.; Noh, H. J.; Kim, J. Y.; Park, J. H.; Hwang, N. M.; Hyeon, T. *Nat. Mater.* **2004**, *3*, 891. (h) Zitoun, D.; Pinna, N.; Frolet, N.; Belin, C. *J. Am. Chem. Soc.* **2005**, *127*, 15034.
(21) (a) Rietveld, H. M. *Acta Crystallogr.* **1966**, *20*, 508. (b) Young, R. A. *The Rietveld Method*; University Press: Oxford, 1995.
(22) (a) Lutterotti, L.; Gialanella, S. *Acta Mater.* **1997**, *46*, 101. (b) Sort, J.; Zhilyaev, A.; Zielinska, M.; Nogués, J.; Suriñach, S.; Thibault, J.; Baró, M. D. *Acta Mater.* **2003**, *51*, 6385.

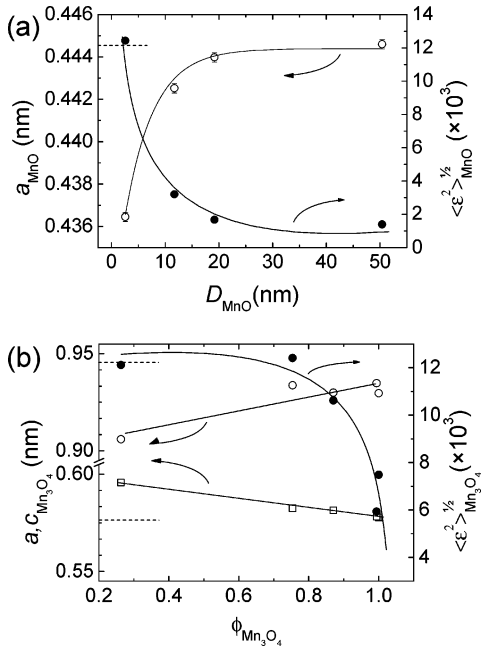

Figure 2. (a) Variation of the MnO cubic crystal lattice parameter, a_{MnO}, and its microstrain, $\langle \epsilon^2 \rangle^{1/2}_{MnO}$, with the MnO particle diameter, D_{MnO}. (b) Variation of the Mn_3O_4 lattice cell parameters, $a_{Mn_3O_4}$ (□) and $c_{Mn_3O_4}$ (○), and its microstrain, $\langle \epsilon^2 \rangle^{1/2}_{Mn_3O_4}$, with the Mn_3O_4 volume fraction, $\phi_{Mn_3O_4}$. The dashed lines show the values found in bulk, while the solid lines are guides to the eye.

and narrowing of the peaks corresponding to the cubic MnO phase which is associated with an increase of the volume fraction and size of the cubic phase, ϕ_{MnO}, and a decrease of the tetragonal Mn_3O_4 volume fraction, $\phi_{Mn_3O_4}$, when going from sample S1 to S5. The data obtained from the XRD analysis are presented in Table 1, together with the particle (crystallite) sizes determined from the Lorentzian contribution to the peak broadening. The table shows that the crystallite size of the tetragonal Mn_3O_4 phase, $t_{Mn_3O_4}$, is 5−6 nm and remains practically the same for all the samples. Analysis of the surface composition of the particles with XPS showed the presence of Mn(II) and Mn(III)[23] (see Supporting Information). These results are consistent with the passivation of the particles in air;[12,20a] namely, Mn_3O_4 forms a shell with a thickness of about $t_{Mn_3O_4} \approx 6$ nm on the MnO nanoparticle cores. Hence, since the thickness of the Mn_3O_4 phase remains constant, we will express the results in terms of the crystallite diameter of the MnO phase, D_{MnO}. Note that some of the measurements were repeated several months after the initial study, rendering virtually the same results, which confirms the stability of the samples, in contrast with metallic core−shell nanoparticles.[24]

Due to the contact between the two crystallographic phases with very different lattice parameters, it is expected that there is certain strain at the interface. Figure 2a shows that the cubic lattice cell parameter for MnO, a_{MnO}, increases with the core size, D_{MnO}, until it reaches the value reported for the bulk (JCPDS Card No. 07-0230). The contraction of the cell parameter a_{MnO} for small D_{MnO} resulted in an increase of the lattice microstrain, reaching values in excess of 1%. Similarly, the lattice cell parameters corresponding to the Mn_3O_4 tetragonal phase, $a_{Mn_3O_4}$ and $c_{Mn_3O_4}$, varied dramatically (ca. 3%) with the volume fraction, $\phi_{Mn_3O_4}$, as shown in Figure 2b. The values also tend to stabilize as the particle becomes mainly Mn_3O_4, with values similar to those found in the bulk (JCPDS Card No. 24-0734). The effect of such changes in the Mn_3O_4 lattice parameters is also reflected in the microstrain, $\langle \epsilon^2 \rangle^{1/2}_{Mn_3O_4}$, which decayed rapidly with increasing $\phi_{Mn_3O_4}$ from about 1.2% to less than 0.6%. Note that the observed values for $\langle \epsilon^2 \rangle^{1/2}_{Mn_3O_4}$ remained somewhat larger that those obtained for $\langle \epsilon^2 \rangle^{1/2}_{MnO}$ due to the much smaller crystallite size.

Figure 3a−e shows TEM micrographs of the as-synthesized core−shell particles with average sizes ranging from about 5

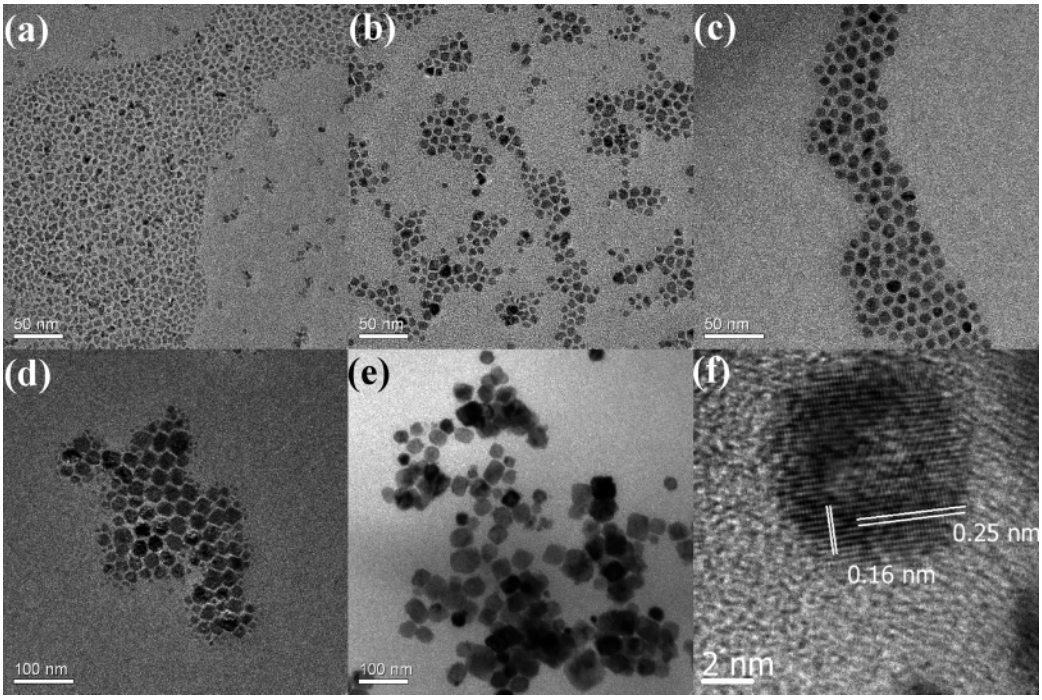

Figure 3. TEM micrographs of samples (a) S1, (b) S2, (c) S3, (d) S4, and (e) S5, as described in Table 1, and (f) a HRTEM image of S2. The lattice fringes of 0.16 and 0.25 nm correspond to either the reflections (220) and (111) of MnO or (224) and (211) of the Mn_3O_4, respectively. Note that the scale bar in (a)−(c) is 50 nm, whereas that in (d) and (e) is 100 nm.

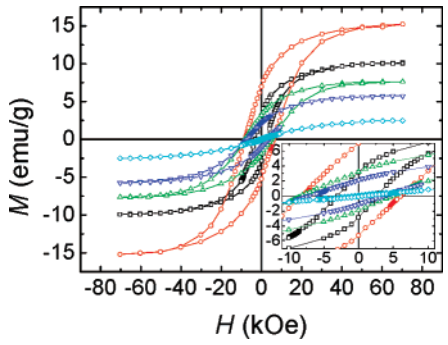

Figure 4. Hysteresis loops at $T = 10$ K for samples S1 (□), S2 (○), S3 (△), S4 (▽), and S5 (◇) cooled under a static field, $H_{FC} = 50$ kOe, from 150 K. The insets show magnified views of the central portion of the loops.

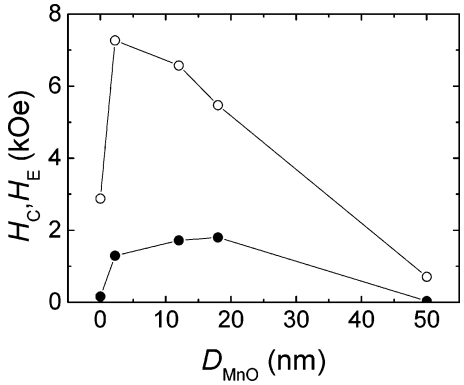

Figure 5. Variation of the coercivity, H_C (○), and the loop shift, H_E (●), measured at 10K after field cooling ($H_{FC} = 50$ kOe) with the core diameter, D_{MnO}. The lines are guides to the eye.

to 60 nm. The synthesized particles were spheroidal, with a narrow size distribution (i.e., $\sigma_P < 20\%$). The spacing between the particles of about 1 nm is due to the coating of the particles with oleylamine. The similar electronic density of the two different manganese oxide phases did not allow clear differentiation of the core−shell structure of the nanoparticles. High-resolution electron microscopy did not show strong differences either, probably due to the similarity in the lower lattice fringes of the cubic and tetragonal phases (Figure 3f). However, since the passivation of the particle occurs from the surface inward, we can assume that the crystallographic domains observed near the edges of the particles correspond to the Mn_3O_4 tetragonal phase. The particle sizes obtained with TEM, D_P, correspond roughly to the sum of the core diameter and twice the shell thickness, i.e., $D_P \approx D_{MnO} + 2t_{Mn_3O_4}$ (for sample S1, $D_P \equiv t_{Mn_3O_4}$), confirming the passivation shell structure.

Figure 4 shows the hysteresis loops recorded at 10 K for the different samples cooled from 150 K under an applied static field $H_{FC} = 50$ kOe. The high-field susceptibility has been subtracted from all the hysteresis loops. The enhanced coercivity values, H_C (relative to the sample with no MnO core), and the loop shift along the field axis, H_E, displayed by all the loops are indicative of the exchange coupling between the ferrimagnetic shell, composed of Mn_3O_4, and the antiferromagnetic core, composed of MnO. Note that the vertical shift detected in all the samples is negligibly small. Moreover, when the samples are zero-field-cooled (not shown), the loops are centered about the origin.

From the analysis of the hysteresis loops, it can be seen that there is a non-monotonic behavior of H_C and H_E, as shown in Figure 5. The coercivity, H_C, of the particles increases dramatically between the sample with no MnO core (sample S1, $H_C = 2.8$ kOe) and the sample with the smallest core (S2, $D_{MnO} = 2.2$ nm, with a maximum of nearly $H_C = 7.2$ kOe). H_C then decreases as the core size is further increased. Similarly, the loop shift (exchange bias) also exhibits a peak as a function of D_{MnO}. However, in this case, the maximum appears for a core size of $D_{MnO} = 18$ nm, with $H_E = 1.8$ kOe. As the measuring temperature is increased, both H_C and H_E quickly decrease, vanishing in all cases toward 50 K (see Supporting Information).

Discussion

Controlling the reaction conditions allows for the synthesis of MnO nanocrystals in a wide size range with average diameters from ~5 to ~60 nm. The growth of spherical nanoparticles can be modeled[20a] using the Lifshitz−Slyozov−Wagner approach.[25] It is assumed that the growth is the slowest step, and it is determined by the diffusion of solute occurring from particles smaller than a critical size D_0 to the larger particles:[26]

$$D^3 - D_0^3 = \frac{64\gamma\Lambda\bar{V}^2 c_\infty}{9RT}\tau \qquad (1)$$

where D is the particle diameter at time τ, γ is the surface energy of the solid, Λ is the diffusion of solute across the grain boundary, $\bar{V}$ is the molar volume, c_∞ is the solubility at a flat surface, and R is the universal gas constant. From (1) it can be seen that, for a given system, the radius (diameter) of a particle will increase as the residence time at a given temperature increases. This can be seen in samples S1−S3, which were prepared under similar [S]:[M] conditions, albeit with increasing temperature and time. Particles larger than those obtained in sample S3 could not be prepared under [S]:[M] = 20 conditions by mere use of longer residence times, which resulted in highly faceted particles (not shown). However, the last condition to be adjusted was the surfactant-to-metal molar ratio. Samples S4 and S5 were prepared with a [S]:[M] 10 times lower than that of sample S3. The particle size was shown to be dominated by the growth (Ostwald ripening) of the particles, so use of a larger concentration of solute allowed for the preparation of particles with the largest size (sample S5), which was prepared using a ~70% increase of metal precursor with respect to that used for sample S4. The subsequent exposure to air resulted in surface passivation of the particles to generate the core−shell structure.

With regard to the magnetic properties of the pure Mn_3O_4 nanoparticles, interestingly, they exhibit a rather large coercivity, $H_C = 2.8$ kOe. Actually, large coercivities have been already observed in Mn_3O_4 bulk, thin films, nanoparticles, and

(23) (a) Langell, M. A.; Hutchings, C. W.; Carson, G. A.; Nassir, M. H. *J. Vac. Sci. Technol. A* **1996**, *14*, 1656. (b) Kurata, H.; Colliex, C. *Phys. Rev. B* **1993**, *48*, 2102. (c) Oku, M.; Hirokawa, K.; Ikeda, S. *J. Electron Spectrosc. Relat. Phenom.* **1975**, *7*, 465.
(24) (a) Cho, S.-J.; Idrobo, J.-C.; Olamit, J.; Liu, K.; Browning, N. D.; Kauzlarich, S. M. *Chem. Mater.* **2005**, *17*, 3181. (b) Cho, S.-J.; Shahin, A. M.; Long, G. J.; Davies, J. E.; Liu, K.; Grandjean, F.; Kauzlarich, S. M. *Chem. Mater.* **2005**, *18*, 960.
(25) (a) Lifshitz, I. M.; Slyosov, V. V. *J. Phys. Chem. Solid* **1961**, *19*, 35. (b) Wagner, C. *Z. Elektrochem.* **1961**, *65*, 581. (c) Ozkam, G. *J. Sol-Gel Sci. Technol.* **2006**, *37*, 161.
(26) (a) Cushing, B. L.; Kolesnichenko, V. L.; O'Connor, C. J. *Chem. Rev.* **2004**, *104*, 3893. (b) Peng, X.; Wickham, J.; Alivisatos, A. P. *J. Am. Chem. Soc.* **1998**, *1210*, 5343.

nanowires[19e,g,27−29] and are expected due to the rather strong anisotropy of Mn_3O_4, $K_{Mn_3O_4} = 1.4 \times 10^6$ erg/cm^3.[27] The Mn_3O_4 nanoparticles also exhibit a moderate exchange bias, $H_E = 160$ Oe. This is actually the first report of loop shifts in Mn_3O_4, which arise from the exchange coupling of the disordered surface spins (spin-glass-like) to the ferrimagnetically ordered core spins.[3] In fact, due to its large anisotropy, Mn_3O_4 is expected to display small exchange bias that is only observable for very small nanoparticles (note that 4.8 nm is among the smallest Mn_3O_4 nanoparticles reported so far[19f,20f]), since the large bulk anisotropy overwhelms any surface effect. This effect is similar to what is observed for nanoparticles of $CoFe_2O_4$ with a high anisotropy, which exhibit weaker surface effects[30] (and only observable for very small nanoparticles) than, for example, nanoparticles of γ-Fe_2O_3 with a low anisotropy, which show large surface canting or large exchange bias.[20g,31,32]

In relation to the MnO−Mn_3O_4 nanoparticles, it is noteworthy that the unusual magnetic structure AFM-core|FiM-shell, contrary to the common FM-core|AFM-shell, actually allows us to systematically address the effect of the size of AFM counterpart (rather than the FM size, as is typically studied[3]). Another unusual feature of the MnO−Mn_3O_4 system is the fact that $T_C(Mn_3O_4) \approx 43$ K $< T_N(MnO) \approx 122$ K.[27,33] Although in exchange-biased systems it is commonly assumed that T_C of the FM layer has to be larger than T_N during the field-cooling procedure,[6] it has been demonstrated in thin-film systems that exchange bias can be induced in systems with $T_C < T_N$. Namely, the magnetization in the paramagnetic (PM) state induced by the cooling field, and probably some local ordering of the PM at the interface due to the AFM, are sufficient to induce exchange bias.[34] However, our system with a high-anisotropy FiM and a low-anisotropy AFM[35] ($K_{MnO} = 3.2 \times 10^4$ erg/cm^3), cannot be directly compared with systems such as amorphous FeNiB−CoO (low K_{FM}, high K_{AFM}).[34] In fact, some bilayer systems which contain MnO as the antiferromagnet exhibit exchange bias.[36] However, the loop shift observed in bilayer systems,[36] in ball-milled FM−MnO materials,[37] or in MnO embedded in a Co matrix[38] is considerably smaller than the one observed in MnO−Mn_3O_4 core−shell particles. Actually, if the interface energy, ΔE (for thin films $\Delta E = H_E t_{FM} M_S$, where t_{FM} and M_S are the FM thickness and the saturation magnetization, respectively), is calculated, the apparent large difference between the two types of systems becomes smaller; i.e., for films, $\Delta E \approx 0.002-0.009$ erg/cm^2 (at 10 K), while for nanoparticles with $\langle D \rangle_{MnO} = 18$ nm, $\Delta E \approx 0.05$ erg/cm^2 (at 10 K). Note that, for core−shell nanoparticles, the expression used for thin films has to be modified to represent the effective geometrical thickness of the ferromagnetic component, $t'_{FM} = V_S/A_C$, where V_S and A_C represent the volume of the ferromagnetic shell and the interface area, respectively. The volume of the shell is calculated as $V_S = (\pi/6)(D_P^3 - D_C^3)$, and assuming the particle size $D_P = D_C + 2t_S$, then $V_S = (\pi/6)[(D_C + 2t_S)^3 - D_C^3]$. Hence, using an interface area $A_C = \pi D_C^2$, the effective thickness is

$$t'_{FM} = \frac{V_S}{A_C} = \frac{[(D_C + 2t_S)^3 - D_C^3]}{6D_C^2} \qquad (2)$$

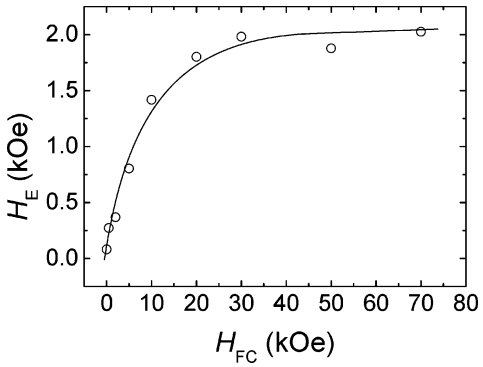

Figure 6. Variation of loop shift, H_E, at 10 K with field cooling, H_{FC}, for sample S4 (with $D_{MnO} = 18$ nm). The line is a guide to the eye.

Exchange bias has also been observed in nominally pure MnO nanoparticles, with H_E values in the range of 500 Oe.[39] However, although this effect probably still exists to some extent in the core−shell nanoparticles, the surface of the MnO cores is now covered by Mn_3O_4, and thus the nature of the surface disordered spins, i.e., the origin of exchange bias in AFM nanoparticles, is different since they are strongly exchange-coupled to the FiM Mn_3O_4.

Further evidence for a "true" FiM−AFM exchange coupling (rather than only surface effects) arises from the dependence of H_E on the cooling field, H_{FC}. As can be seen in Figure 6, H_E increases with H_{FC}, saturating for H_{FC} larger than ~30−50 kOe. This behavior is reminiscent of that observed for FM−AFM bilayers with $T_C < T_N$[34] and is in contrast to that observed for systems involving spin-glass types of phases, which typically show a decrease of H_E for large H_{FC}.[40] Similarly, as can be seen in Figure 7, when the maximum applied field, H_{max}, during the hysteresis loop is exceedingly low, the loops exhibit large horizontal and vertical (V_{shift}) shifts. However, for large H_{max}, H_E stabilizes while V_{shift} virtually vanishes. These results are consistent with minor loop effects and are opposite to those observed for systems with spin-glass phases, which exhibit large V_{shift}. Moreover, the training effect (i.e., the reduction of H_E

(27) Dwight, K.; Menyuk, N. *Phys. Rev.* **1960**, *119*, 1470.
(28) Guo, L. W.; Peng, D. L.; Makino, H.; Inaba, K.; Ko, H. J.; Sumiyama, K.; Yao, T. *J. Magn. Magn. Mater.* **2000**, *213*, 321.
(29) (a) Winkler, E.; Zysler, R. D.; Fiorani, D. *Phys. Rev. B* **2004**, *70*, 174406. (b) Sun, X.; Zhang, Y. W.; Si, R.; Yan, C. H. *Small* **2005**, *1*, 1081.
(30) (a) Moumen, N.; Pileni, M. P. *J. Phys. Chem.* **1996**, *100*, 1867. (b) Ngo, A. T.; Bonville, P.; Pileni, M. P. *J. Appl. Phys.* **2001**, *89*, 3370.
(31) Coey, J. M. D. *Phys. Rev. Lett.* **1971**, *27*, 1140.
(32) Martinez, B.; Obradors, X.; Balcells, Ll.; Rouanet, A.; Monty, C. *Phys. Rev. Lett.* **1998**, *80*, 181.
(33) (a) Shull, C. G.; Smart, J. S. *Phys. Rev.* **1949**, *76*, 1256. (b) Shull, C. G.; Strauser, W. A.; Wollan, E. O. *Phys. Rev.* **1951**, *83*, 333.
(34) (a) Wu, X. W.; Chien, C. L. *Phys. Rev. Lett.* **1998**, *81*, 2795. (b) Cai, J. W.; Liu, K.; Chien, C. L. *Phys. Rev. B* **1999**, *60*, 72.
(35) Keffer, F.; O'Sullivan, W. *Phys. Rev.* **1957**, *108*, 637.
(36) (a) Ge, Z.; Lim, W. L.; Shen, S.; Zhou, Y. Y.; Liu, X.; Furdyna, J. K.; Dobrowolska, M. *Phys. Rev. B* **2007**, *75*, 014407. (b) Dziatkowski, K.; Ge, Z.; Liu, X.; Furdyna, J. K. *Appl. Phys. Lett.* **2006**, *88*, 142513. (c) Eid, K. F.; Stone, M. B.; Maksimov, O.; Shih, T. C.; Ku, K. C.; Fadgen, W.; Palmstrøm, C. J.; Schiffer, P.; Samarth, N. *J. Appl. Phys.* **2005**, *97*, 10D304. (d) Eid, K. F.; Stone, M. B.; Ku, K. C.; Maksimov, O.; Schiffer, P.; Samarth, N.; Shih, T. C.; Palmstrøm, C. J. *Appl. Phys. Lett.* **2004**, *85*, 1556. (e) Liu, H. X.; Wu, S. Y.; Singh, R. K.; Newman, N. *J. Appl. Phys.* **2005**, *98*, 046106.
(37) (a) Hernández Padrón, E.; Romero, S. A.; Rechenberg, H. R.; Rezende, S. M.; Cornejo, D. R. *J. Alloys Compd.* **2004**, *369*, 269. (b) Cornejo, D. R.; Padrón Hernández, E.; Azevedo, A.; Rezende, S. M. *J. Appl. Phys.* **2005**, 97, 10K103.
(38) van Lierop, J.; Schofield, M. A.; Lewis, L. H.; Gambino, R. J. *J. Magn. Magn. Mater.* **2003**, *264*, 146.
(39) Zhang, H. T.; Chen, X. H. *J. Phys. Chem. B* **2006**, *110*, 9442.
(40) (a) del Bianco, L.; Fiorani, D.; Testa, A. M.; Bonetti, E.; Signorini, L. *Phys. Rev. B* **2004**, *70*, 052401. (b) Wang, H.; Zhu, T.; Zhao, K.; Wang, W. N.; Wang, C. S.; Wang, Y. J.; Zhan, W. S. *Phys. Rev. B* **2004**, *70*, 082409.

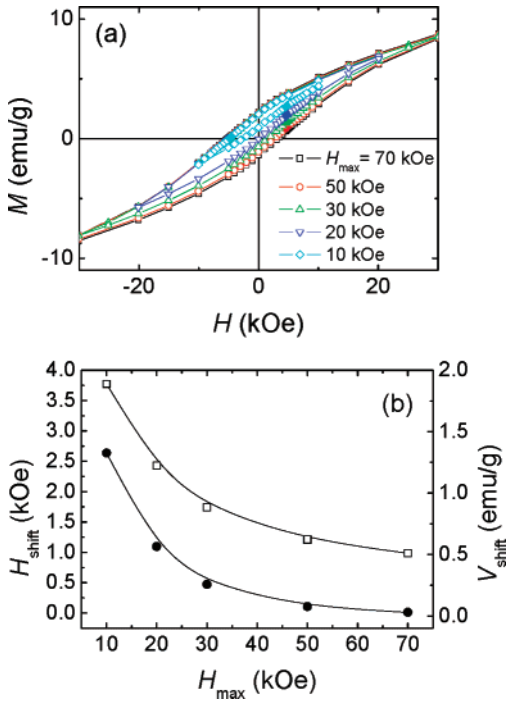

Figure 7. (a) Hysteresis (minor) loops for sample S4 (with $D_{MnO} = 18$ nm) measured at 10K and (b) the corresponding horizontal (□) and vertical (●) loop shifts after field cooling ($H_{FC} = 10$ kOe) using various maximum fields, H_{max}. Note that the hysteresis loops have not been corrected for the high-field susceptibility. The lines are guides to the eye.

with the measurement of consecutive hysteresis loops[41]) is rather weak after a relative large change between the first and second loops. This effect is expected for FM−AFM coupling,[6] although it is commonly larger for systems with spin-glass layers.[32] Finally, note that the AFM nature of the MnO core has been confirmed by neutron diffraction.[42]

Concerning the non-monotonic dependence of H_E on D_{MnO}, although in bilayers the dependence of H_E on the thickness of the AFM usually exhibits a sharp increase above a critical thickness as the AFM becomes thicker, saturating for larger thickness,[43] some systems exhibit a gradual decrease of H_E (after the sharp increase) with increasing AFM thickness[44] (similar to what is observed in our case). This behavior is commonly ascribed to the role of AFM domains,[44,45] where as the AFM becomes thicker the number of domains decreases. Namely, for thicker AFMs, the larger energy necessary to create longer domain walls is not compensated by the gain in entropy of having more domains, and thus the number of domains decreases, reducing the number of uncompensated spins linked to such AFM domains. The decrease in uncompensated spins leads to a reduction of H_E.[44] For the core−shell nanoparticles, due to the cubic character of the anisotropy of MnO,[33] S- or T-type domains could be created in the AFM core,[33b] despite the low AFM anisotropy of MnO. Thus, the presence of AFM domains in the core could explain some of the features observed in the MnO−Mn_3O_4 nanoparticles, using an argument analogous to the one developed for bilayer systems. As domains are created in the core, H_E should increase, since more uncompensated spins would be available. However, as the core becomes larger, the energy needed to create domain walls becomes unfavorable, and thus the number of domains would decrease with the concomitant reduction of H_E.

In fact, in antiferromagnetic nanoparticles, it is well known that, due to finite size effects, defects, or thermally induced spin waves, there is always certain uncompensation of the magnetic lattice, also giving rise to uncompensated spins.[46−48] It is noteworthy that it has been demonstrated in thin films and core−shell nanoparticles that uncompensated spins, from either AFM domains[49] or structural effects,[50] are closely linked to exchange bias.[51,52] Based on the simplest model to explain exchange bias,[6,53] one gets $\Delta E = J_{Int} S_{FM} S_{AFM}$, where J_{Int} is the exchange coupling at the interface and S_{AFM} and S_{FM} are the spins of the AFM and the FM, respectively.[6] However, if we assume that only the uncompensated spins contribute to the bias,[50] the above formula has to be corrected by the amount of uncompensated spins, n, yielding $\Delta E = nJ_{Int} S_{FM} S_{AFM}$. In our system, since the FiM shell is kept roughly constant and the nature of the core remains unchanged, J_{Int}, S_{FM}, and S_{AFM} will be unaltered in the different nanoparticles, and only n will come into play. Assuming only finite size effects, the amount of uncompensated spins distributed over the whole nanoparticle, n, per total number of magnetic ions in the nanoparticle, N, is $n = 1/N^{1/2}$.[46] Thus, since the total number of atoms in a nanoparticle scales with D^3, the number of available uncompensated spins decreases drastically as the size increases, going from $n = 6.2 \times 10^{-2}$ for $\langle D\rangle_{MnO} = 2.2$ nm (~256 Mn(II) ions) to $n = 0.06 \times 10^{-2}$ for $\langle D\rangle_{MnO} = 50$ nm (~3×10^6 Mn(II) ions). Moreover, assuming that only the interface uncompensated spins contribute to H_E, the effect would be even more severe. Consequently, one would expect a reduction in H_E as the size of the core increases, as is indeed observed experimentally for large cores. Interestingly, by using realistic values, e.g., J_{Int} similar to the exchange interactions between Mn atoms in MnO[54] or Mn_3O_4, i.e., $J_{Int} \approx J_{Mn-Mn}/(a_{MnO})^2 = 1.44$ erg/cm^2, $S_{FM} = 2.5$, $S_{AFM} = 2$, $M_{FM} \approx 120$ emu/cm^3 and $t'_{FM} \approx 98$ nm, and using the n value obtained for $\langle D\rangle_{MnO} = 2.2$ nm, corrected for the number of interface spins, a value of $H_E = nJ_{Int} S_{FM} S_{AFM}/M_{FM} t'_{FM} \approx 0.3$ kOe is obtained, which leads to the correct order of magnitude for H_E. However, although this effect could explain the reduction of H_E for large D_{MnO}, the initial increase of H_E for small D_{MnO} must have another origin. In this case, the nanoparticles should exhibit an effect similar to that observed in bilayer films; i.e., when the

(41) (a) Hoffmann, A. *Phys. Rev. Lett.* **2004**, *93*, 097203. (b) Schlenker, C.; Paccard, D. *J. Phys. (Paris)* **1967**, *28*, 611.
(42) Salazar-Alvarez, G.; Sort, J.; Nogués, J. ILL Report CRG-1180, 2006.
(43) (a) Lund, M. S.; Macedo, W. A. A.; Liu, K.; Nogués, J.; Schuller, I. K.; Leighton, C. *Phys. Rev. B* **2002**, *66*, 054422. (b) Ambrose, T.; Chien, C. L. *J. Appl. Phys.* **1998**, *83*, 6822.
(44) (a) Ali, M.; Marrows, C. H.; Al-Jawad, M.; Hickey, B. J.; Misra, A.; Nowak, U.; Usadel, K. D. *Phys. Rev. B* **2003**, *68*, 214420. (b) Baltz, V.; Sort, J.; Landis, S.; Rodmacq, B.; Dieny, B. *Phys. Rev. Lett.* **2005**, *94*, 117201.
(45) Malozemoff, A. P. *Phys. Rev. B* **1988**, *37*, 7673.
(46) (a) Néel, L. *C. R. Acad. Sci.* **1961**, *252*, 4075. (b) Richardson, J. T.; Yiagas, D. I.; Turk, B.; Foster, K.; Twigg, M. V. *J. Appl. Phys.* **1991**, *70*, 6977.
(47) Tracy, J. B.; Bawendi, M. G. *Phys. Rev. B* **2006**, *74*, 184434.
(48) Madsen, D. E.; Mørup, S. *Phys. Rev. B* **2006**, *74*, 014405.
(49) Miltényi, P.; Gierlings, M.; Keller, J.; Bescherten, B.; Güntherodt, G.; Nowak, U.; Usadel, K. D. *Phys. Rev. Lett.* **2000**, *84*, 4224.
(50) Takano, K.; Kodama, R. H.; Berkowitz, A. E.; Cao, W.; Thomas, G. *Phys. Rev. Lett.* **1997**, *79*, 1130.
(51) (a) Nogués, J.; Leighton, C.; Schuller, I. K. *Phys. Rev. B* **2000**, *61*, 1315. (b) Hoffmann, A.; Seo, J. W.; Fitzsimmons, M. R.; Siegwart, H.; Fompeyrine, J.; Locquet, J. P.; Dura, J. A.; Majkrzak, C. F. *Phys. Rev. B* **2002**, *66*, 220406. (c) Roy, S.; Fitzsimmons, M. R.; Park, S.; Dorn, M.; Petracic, O.; Roshchin, I. V.; Li, Z. P.; Batlle, X.; Morales, R.; Misra, A.; Zhang, X.; Chesnel, K.; Kortright, J. B.; Sinha, S. K.; Schuller, I. K. *Phys. Rev. Lett.* **2005**, *95*, 047201.
(52) Zheng, R. K.; Wen, G. H.; Fung, K. K.; Zhang, X. X. *J. Appl. Phys.* **2004**, *95*, 5244.
(53) (a) Meiklejohn, W. H.; Bean, C. P. *Phys. Rev.* **1957**, *105*, 904. (b) Meiklejohn, W. H. *J. Appl. Phys.* **1962**, *33*, 1328.
(54) Oguchi, T.; Terakura, K.; Williams, A. R. *Phys. Rev. B* **1983**, *28*, 6443.

anisotropy energy of the AFM, i.e., $K_{MnO}V_{MnO}$ (where V_{MnO} is the volume of the core) becomes exceedingly small for reduced D_{MnO}, the AFM spins can no longer remain pinned and are dragged by the FiM as its magnetization reverses, leading to a reduction of H_E.[6] However, due to the intrinsic H_E of the Mn_3O_4 shell, the transition of $H_E(D_{MnO})$ becomes broader than what is usually observed in bilayers[43,44] and actually does not reach $H_E(D_{MnO}\rightarrow 0) = 0$. Surprisingly, despite the low anisotropy of MnO, a core of $D_{MnO} = 2.2$ nm is still capable of inducing exchange bias, probably due to the magnetic stabilization of MnO by the highly anisotropic Mn_3O_4 shell.

Regarding the dependence of the coercivity on D_{MnO}, arguments similar to the ones put forward for the dependence of H_E on D_{MnO} can be applied. However, the change of coercivity is somewhat more complex, since the drastic change of H_C has two main origins: (i) the AFM−FiM exchange coupling and (ii) a change in geometry of the FiM. Namely, Mn_3O_4 goes from being a spherical particle to being a spherical crown (i.e., a shell); thus, the magnetization reversal modes will inevitably change, which could affect the coercivity of the system.[55] In any case, it is expected that, as H_E starts to rise with increasing D_{MnO}, H_C should have a peak at low D_{MnO} (low $K_{MnO}V_{MnO}$), since the dragging of the AFM spins by the FiM shell should dramatically increase H_C,[6,56] as is observed experimentally. Then, as the spins of the AFM become increasingly pinned (higher $K_{MnO}V_{MnO}$ for larger D_{MnO}) and fewer spins are dragged by the FiM shell, the coercivity should decrease, in qualitative agreement with the experimental results. It is noteworthy that the existence of the surfactant covering the MnO|Mn_3O_4 nanoparticle avoids spurious effects originating from possible shell−shell interactions.[57] Note also that the presence of domains in the core could also have a strong effect on H_C.[42,58]

It should be taken into account that other effects could play some role in the magnetic properties of the core−shell nanoparticles. Explicitly, one has to recall the fact that the Néel temperature of MnO ($T_N = 122$ K)[33] is higher than the Curie temperature of Mn_3O_4 ($T_C = 43$ K).[27] If MnO particles are large enough, their transition temperature will thus be higher than the transition temperature of Mn_3O_4 shells. In this case, during the field-cooling process, the antiferromagnetic order in MnO will be set before Mn_3O_4 becomes ferrimagnetic. It has been shown for thin films that, typically in this case, the obtained H_E is smaller than for the common $T_N < T_C$ case.[34] Conversely, when the MnO cores are reduced in size, the blocking temperature of MnO is progressively shifted toward lower values, and eventually the antiferromagnetic order will be set in a temperature range similar to (or lower than) that of the ferrimagnetic order in Mn_3O_4. In this case, the spins in Mn_3O_4 will be oriented with the field when the AFM order in MnO is set, and a larger coupling will appear. Actually, the microscopic origin of the exchange bias effect in this system should be rather complex and probably involves more than one of the above-described processes.

As for the temperature dependence of H_E and H_C, both quantities vanish much below the bulk T_N of MnO. Actually, H_E and H_C become zero close to the T_C of Mn_3O_4. This is in contrast with what is observed in bilayers with $T_C < T_N$, where $H_E \neq 0$ is observed even above T_C.[34] However, as discussed earlier, these systems are composed of large K_{AFM} and small K_{FM}. In our case, since the FiM layer has a much larger anisotropy than the AFM, it is the former that dictates the temperature dependence of the exchange bias temperatures, as is indeed observed for FM−MnO bilayers.[36]

Conclusions

Summarizing, MnO-core|Mn_3O_4-shell nanoparticles with a narrow size distribution were prepared with average sizes in a wide range by the thermal decomposition of metal salts in organic precursors to fabricate the MnO cores and their corresponding passivation to render the Mn_3O_4 shell. The inverse core−shell structure, namely antiferromagnetic core−ferrimagnetic shell, allowed their magnetic properties to be investigated as a function of the core (antiferromagnet) size, D_{MnO}. The coercivity of the particles showed a non-monotonic dependence on D_{MnO}. Furthermore, upon field cooling, the particles displayed a loop shift along the field axis, i.e., exchange bias due to the coupling of the weakly anisotropic MnO antiferromagnetic core and the highly anisotropic Mn_3O_4 ferrimagnetic shell with a $T_C < T_N$. The dependence of the magnetic properties on the core size was explained in terms of the magnetic coupling of the highly anisotropic Mn_3O_4 shell and the antiferromagnetic MnO core and size effects in the latter.

Acknowledgment. This work is supported by the Spanish CICYT (MAT2004-01679 and MAT2007-66302-C02), MEC (CSD2006-00012 Consolider-Ingenio 2010), the Catalan DGR (2005-SGR-00401), and the Institut Català de Nanotecnologia. The authors thank the Serveis de Microscòpia and d'Anàlisi Química at UAB for technical assistance.

Supporting Information Available: XPS spectra of the samples at the Mn 2p edge and temperature dependence of the coercivity and loop shift on the core size. This material is available free of charge via the Internet at http://pubs.acs.org.

JA0714282

(55) Goll, D.; Berkowitz, A. E.; Bertram, H. N. *Phys. Rev. B* **2004**, *70*, 184432.
(56) Leighton, C.; Fitzsimmons, M. R.; Hoffmann, A.; Dura, J.; Majkrzak, C. F.; Lund, M. S.; Schuller, I. K. *Phys. Rev. B* **2002**, *65*, 064403.
(57) Nogués, J.; Skumryev, V.; Sort, J.; Givord, D. *Phys. Rev. Lett.* **2006**, *97*, 157203.
(58) Leighton, C.; Nogués, J.; Jönsson-Åkerman, B. J.; Schuller, I. K. *Phys. Rev. Lett.* **2000**, *84*, 3466.